Deficiency of gluconeogenic enzyme PCK1 promotes murine NASH progression and fibrosis by activation PI3K/AKT/PDGF axis

Qian Ye[1,#], Yi Liu[1,#], Guiji Zhang[1,#], Haijun Deng[1,#], Xiaojun Wang[2,#], Chang Chen[3], Xuanming Pan[1], Kang Wu[1], Jiangao Fan[4], Qin Pan[4], Kai Wang[1,*], Ailong Huang[1,*], Ni Tang[1,*]

[1]Key Laboratory of Molecular Biology for Infectious Diseases (Ministry of Education), Institute for Viral Hepatitis, Department of Infectious Diseases, The Second Affiliated Hospital, Chongqing Medical University, Chongqing, China

[2]Institute of Hepatobiliary Surgery, Southwest Hospital, Third Military Medical University (Army Medical University), Chongqing, China

[3]Institute of Life Sciences, Chongqing Medical University, Chongqing, China

[4]Department of Gastroenterology, Xin Hua Hospital, School of Medicine, Shanghai Jiao Tong University, Shanghai, China

[#]These authors contributed equally to this work.

***Corresponding author:** Ni Tang, Ailong Huang, Kai Wang, Key Laboratory of Molecular Biology for Infectious Diseases (Ministry of Education), Institute for Viral Hepatitis, Department of Infectious Diseases, The Second Affiliated Hospital, Chongqing Medical University, Chongqing 400016, China. Tel: 86-23-68486780, Fax: 86-23-68486780, E-mail: nitang@cqmu.edu.cn (N.T.), ahuang@cqmu.edu.cn (A.H.), wangkai@cqmu.edu.cn (K.W.)

Abstract:

Background and Aims:

Nonalcoholic steatohepatitis (NASH) is a chronic liver disease characterized by hepatic lipid accumulation, inflammation, and progressive fibrosis. However, the pathomechanisms underlying NASH are incompletely explored. Phosphoenolpyruvate carboxykinase 1 (PCK1) catalyzes the first rate-limiting step of gluconeogenesis. This study was designed to determine the role of PCK1 in regulating NASH progression.

Methods:

Liver metabolism, hepatic steatosis, and fibrosis were evaluated at 24 weeks in liver-specific *Pck1*-knockout mice fed with NASH diet or chow diet. Gain- or loss-of-function approaches were used to explore the underlying mechanism *in vitro*. AKT and RhoA inhibitors were evaluated for NASH treatment *in vivo*.

Results:

Hepatic PCK1 was downregulated in patients with NASH and mouse models of NASH. Mice with liver *Pck1* deficiency displayed hepatic lipid disorder and liver injury fed with normal diet, while showed aggravated fibrosis and inflammation when fed NASH diet. Mechanistically, PCK1 deficiency upregulated genes involved in fatty acid transport and lipid droplet formation. Moreover, metabolomics analysis showed the accumulation of glycerol 3-phosphate, the substrate of triglyceride synthesis. Furthermore, the loss of hepatic PCK1 could activate the RhoA/PI3K/AKT pathway, which leads to

increased secretion of PDGF-AA and promotes the activation of hepatic stellate cells. Accordingly, treatment with RhoA and AKT inhibitors alleviated NASH progression in the presence of *Pck1* deletion *in vivo*.

Conclusions:

PCK1 deficiency plays a key role in the development of hepatic steatosis and fibrosis by facilitating the RhoA/PI3K/AKT/PDGF-AA axis. These findings provide a novel insight into therapeutic approaches for the treatment of NASH.

Keywords: phosphoenolpyruvate carboxykinase 1; gluconeogenesis; non-alcoholic steatohepatitis; PI3K/AKT pathway; platelet-derived growth factor AA

Introduction

Non-alcoholic fatty liver disease (NAFLD) is the most common chronic liver disease worldwide affecting nearly 25% of U.S. and European adults.[1] NAFLD is characterized by aberrant lipid accumulation in hepatocytes in the absence of excessive alcohol consumption. NAFLD may progress to non-alcoholic steatohepatitis (NASH), a more serious form of liver damage hallmarked by irreversible pathological changes such as inflammation, varying degrees of fibrosis, and hepatocellular damage, which is more likely to develop into cirrhosis and hepatocellular carcinoma (HCC).[2] Although multiple parallel insults, including oxidative damage, endoplasmic reticulum stress, and hepatic stellate cell (HSC) activation have been proposed to explain the pathogenesis of NASH, the underlying mechanisms remain incompletely elucidated.[3]

Gluconeogenesis is the process of generating glucose from non-carbohydrate substrates such as glycerol, lactate, pyruvate, and glucogenic amino acids, which occurs mainly in the liver to maintain glucose levels and energy homeostasis. Phosphoenolpyruvate carboxykinase 1 (PCK1) is the first rate-limiting enzyme in the gluconeogenesis which converts oxaloacetate (OAA) to phosphoenolpyruvate (PEP) in the cytoplasm.[4] Our previous studies have shown that PCK1 deficiency promotes HCC progression by enhancing the hexosamine-biosynthesis pathway.[5] However, PCK1 has been found to regulate not only glucose homeostasis but also lipogenesis by activating sterol

regulatory element-binding proteins (SREBPs).[6] Patients lacking PCK1 function present diffuse hepatic macrosteatosis concomitant with hypoglycemia and hyperlactacidemia.[7] Likewise, mice with reduced *Pck1* expression develop insulin resistance and exhibit hypoglycemia as well as hepatic steatosis, indicating an important role of PCK1 in regulating both glucose homeostasis and lipid metabolism.[8, 9] However, the exact role of PCK1 during NASH progression is incompletely understood.

The phosphoinositide 3-kinase/protein kinase B (PI3K/ATK) pathway plays a critical role in regulating cell growth and metabolism. This pathway can be activated in response to insulin, growth factors, energy, and cytokines, and in turn, regulates key metabolic processes, including glucose and lipid metabolism, as well as protein synthesis.[10] AKT promotes *de novo* lipogenesis (DNL) primarily through SREBP activation.[11] PI3K/AKT dysregulation leads to many pathological metabolic conditions, including obesity and type 2 diabetes.[12] NAFLD is characterized by disordered glucose and lipid metabolism in liver. Although PI3K/AKT pathway is a key regulator for sensing metabolic stress, its exact role in NAFLD/NASH progression is unclear.[13, 14]

In this study, we explored the role of *Pck1* in a mouse NASH model. We unraveled the molecular mechanisms underlying disordered lipid metabolism, inflammation, and fibrosis induced by *Pck1* depletion. We also delineated the

functional importance of the PI3K/AKT pathway and its effectors in steatohepatitis, providing a potential therapeutic strategy for treating NASH.

Materials and Methods

Animal models.

Pck1$^{loxp/loxp}$ mice with a 129S6/SvEv background were purchased from the Mutant Mouse Resource & Research Centers (MMRRC: 011950-UNC) and *Alb-Cre* mice with a C57BL/6 background were purchased from Model Animal Research Center of Nanjing University. To generate liver-specific *Pck1*-knockout mice (L-KO), *Alb-Cre* mice were crossed with *Pck1*$^{loxp/loxp}$ mice. *Pck1*$^{loxp/loxp}$ mice from the same breeding were used as control (wild-type, WT). Male WT and L-KO mice, 7-9-week-old, were fed NASH diet (Research Diets, D12492: 60% Kcal fat, with drinking water containing 23.1 g/L fructose and 18.9 g/L glucose) (n=11 per group) or a control chow diet (Research Diets, D12450J: 10% Kcal fat, with tap water) (n=10 per group) for 24 weeks. Food and drinking water were provided *ad libitum*. All mice were housed in temperature-controlled (23°C) pathogen-free facilities with a 12-hour light-dark cycle. For the male L-KO mice in the treatment group, after fed with NASH diet for 16 weeks, mice were divided into 3 groups and intraperitoneally (*i.p.*) injected with vehicle solution (n=6), MK2206 (AKT inhibitor, 50 mg/kg, every 3 days) (n=5) or Rhosin (RhoA inhibitor, 20 mg/kg, every 3 days) (n=6) for 8 weeks, respectively. All mice were executed for further study after fed with NASH diet for 24 weeks. Animal experiments were approved by Animal Experimentation Ethics Committees of Chongqing Medical University and were carried out in accordance with the Guide for the Care and Use of

Laboratory Animals.

Liver tissues collection, ELISA, immunoblotting, transcriptomic analyses, untargeted metabolomics, primer sequences, reagents, antibodies, ChIP-qPCR, and other *in vitro* studies are provided in the **Supplementary Materials and Methods.**

Results

PCK1 is downregulated in patients with NASH and mouse models of NASH

To determine whether PCK1 is involved in NAFLD, we first examined hepatic gene expression in a published transcriptome dataset (GEO: GSE126848) containing samples from 14 healthy, 12 obese, 15 NAFLD, and 16 NASH patients.[15] Bioinformatics analysis showed that 32 genes were markedly changed in obesity, NAFLD, and NASH; 12 genes were considerably downregulated and 20 genes were upregulated (Supplementary Figure 1A-C). Notably, *PCK1* was gradually reduced in obesity, NAFLD, and NASH patients (Figure 1A and B). Downregulation of *PCK1* mRNA was also found in a similar dataset (GSE89632) (Figure 1B). Moreover, q-PCR, immunoblotting, and immunohistochemistry (IHC) assays showed that PCK1 expression were dramatically downregulated in liver samples derived from NASH patients and NASH model mice (Figure 1C-E).

Next, palmitic acid (PA) was used to mimic the liver steatosis of NAFLD patients *in vitro*.[16] Cell growth was assessed by CCK8 assay after treatment with different concentration of PA (Supplementary Figure 1D). Interestingly, PCK1 mRNA and protein levels were downregulated in a dose-dependent manner during 24-hour PA stimulation (Figure 1F and G), suggesting that transcription of PCK1 may be inhibited in response to lipid overload. We

screened several known regulators of *PCK1* (Supplementary Figure 1E and F) and determined *ATF3*, a transcriptional repressor of *PCK1,*[17] was upregulated upon PA stimulation (Figure 1H). Similarly, ATF3 expression was remarkably upregulated in liver samples derived from NASH patients and NASH model mice (Supplementary Figure 1G-I). Chromatin immunoprecipitation assays revealed that the binding of ATF3 to *PCK1* promoter was increased by PA administration (Figure 1I). ATF3 knockdown restored the expression of PCK1 in human hepatocytes under PA treatment (Figure 1J). These results indicate that increased lipids caused upregulation of the repressor ATF3, impairing *PCK1* transcription in NASH patients and mouse models.

L-KO mice exhibit a distinct hepatic steatosis phenotype

To explore the role of *Pck1* in fatty liver disease, WT and L-KO mice were fed with chow diet for 24 weeks (Supplementary Figure 2A). From 16 weeks, L-KO mice showed increased body weight compared with WT mice, however, there was no significant difference in the glucose tolerance test (GTT) and insulin tolerance test (ITT) (Supplementary Figure 2B). Moreover, significant hepatomegaly and increased liver weight were observed in L-KO mice (Supplementary Figure 2C). Alanine transaminase (ALT) and aspartate transaminase (AST) levels were higher in L-KO mice, indicating liver injury (Supplementary Figure 2D). In addition, total triglyceride (TG), total cholesterol (TC), and free fatty acids (FFAs) in liver tissues and serum were elevated in

L-KO mice (Supplementary Figure 2E and F). Histochemistry and ELISA showed that L-KO mice exhibited prominent hepatic steatosis and higher levels of TNF-α (Supplementary Figure 2G-I). These data suggest that L-KO mice exhibited a distinct hepatic steatosis phenotype and liver injury even when fed normal chow.

Hepatic loss of *Pck1* promotes inflammation and fibrogenesis in NASH mice

To explore whether an unhealthy diet could exacerbate the pathologic changes in L-KO mice, WT and L-KO mice were fed with high-fat diet with drinking water containing fructose and glucose (NASH diet) for 24 weeks (Figure 2A).[18, 19] From 4 weeks, L-KO mice showed significant weight gain (Figure 2B). GTT and ITT showed that L-KO mice developed a more severe form of glucose intolerance and insulin resistance (Figure 2C and D). L-KO mice had pale and heavier livers (Figure 2E), although there was no significant difference in liver weight ratio (Supplementary Figure 3A). Insulin, AST, ALT, TC, TG, and FFAs were increased in serum or liver homogenates of L-KO mice, suggesting more serious liver injury and lipid metabolism disorder (Figure 2F; Supplementary Figure 3B and C). Analyses of L-KO liver sections revealed increased fat droplets, more severe fibrosis, and greater macrophage infiltration (Figure 2G and H). Furthermore, L-KO mice had higher NAFLD activity score (NAS score), and higher TNF-α and IL-6 levels (Figure 2I and J).

In addition, the expression of inflammatory factors, lipogenic enzymes, and fibrogenesis associated genes were upregulated in L-KO mice (Supplementary Figure 3D-F). In summary, mice lacking hepatic *Pck1* showed substantial liver inflammation and fibrosis when fed NASH diet.

Transcriptomic and metabolomics analyses confirm loss of *Pck1* promotes hepatic lipid accumulation

To comprehensively investigate the role of *Pck1* in NASH, we performed RNA-seq analysis of liver samples from L-KO and WT mice fed normal chow or NASH diet for 24 weeks. Gene ontology analysis indicated that lipid metabolic processes were remarkably upregulated in L-KO mice fed with NASH diet (Figure 3A). Volcano plot showed that genes involved in fatty acid uptake, such as *Slc27a1* and *Cd36*, and lipid droplet synthesis, such as *Cidec* and *Cidea*, were upregulated in response to NASH diet (Figure 3B). Gene Set Enrichment Analysis (GSEA) revealed that the PPAR signaling pathway was prominently upregulated in L-KO mice fed either diet (Figure 3C; Supplementary Figure 4A and B). Several genes selected from the data set were independently validated by q-PCR and immunoblotting and found to be significantly overexpressed in L-KO mice (Figure 3D and E). Furthermore, genes involved in the glycerol 3-phosphate (G3P) pathway were also upregulated in L-KO mice (Figure 3F). Metabolomics analysis showed that compared with WT mice fed NASH diets, L-KO mice had significantly higher

G3P and PA levels (Figure 3G and H). Since G3P is a substrate for TG synthesis and PA is a key intermediate metabolite in DNL, these data suggested that *Pck1* ablation could promote the substrates accumulation for lipid synthesis.

To further examine the function of PCK1 on steatosis *in vitro*, we overexpressed (*PCK1*-OE) using the AdEasy adenoviral vector system and knocked out PCK1 (*PCK1*-KO) using the CRISPR-Cas9 system in human hepatocytes (Supplementary Figure 4C and D), and found that *PCK1*-OE attenuated the accumulation of lipid droplets, whereas *PCK1*-KO facilitated lipid accumulation (Supplementary Figure 4E and F). Collectively, these results suggested that hepatic *Pck1* deficiency leads to lipid accumulation by promoting the expression of lipogenic genes and the accumulation of substrates related to lipid synthesis (Supplementary Figure 4G).

Hepatic *Pck1* deficiency leads to HSC activation via PI3K/AKT pathway

RNA-seq analysis indicated that the PI3K/AKT pathway was also specifically activated in L-KO mice fed NASH diet (Figure 4A and B). Immunoblotting revealed p-AKT (S473) and p-AKT (T308), two activated forms of AKT, and downstream c-MYC were significantly upregulated in L-KO livers (Figure 4C). Consistently, q-PCR also confirmed the high expression of genes related to PI3K/AKT pathway in L-KO mice (Supplementary Figure 5A). Similarly, p-AKT

(S473 and T308) significantly decreased in human *PCK1*-OE cells, but increased in *PCK1*-KO cells after 0.2 mM PA treatment (Figure 4D and E).

To clarify the role of PI3K/AKT pathway activation, transcriptome data were further analyzed. Interestingly, *Col1a1*, *Col3a1,* and *Lama2*, which are primary components of the extracellular matrix (ECM), were upregulated as shown in the heat map of the PI3K/AKT pathway (Supplementary Figure 5B). Moreover, GSEA analysis revealed that ECM-receptor interaction was upregulated in L-KO mice (Supplementary Figure 5C). Since ECM deposition is usually considered as the key event underlying liver fibrosis, we suspected that activation of the PI3K/AKT pathway may promote fibrosis in L-KO mice. Considering HSCs are major ECM secretors, we performed human hepatocyte (MIHA) and HSC (LX-2) co-culture assays (Figure 4F). Interestingly, mRNA levels of *ACTA2* (α-SMA, an HSC activation marker)*, COL1A1,* and *COL3A1* were increased in HSCs co-cultured with *PCK1*-KO cells, but were decreased in HSCs co-cultured with *PCK1*-OE cells (Figure 4G and H). Likewise, COL1A1, COL3A1, and α-SMA expression was increased in liver tissues and primary HSCs of L-KO mice, which was confirmed by IHC analysis of COL3A1 (Figure 4I-K). However, these increases could be partially reversed by MK2206, an AKT inhibitor (Figure 4L and M). Collectively, these data suggested that loss of PCK1 in hepatocytes induces HSCs activation and ECM formation via activating the PI3K/AKT pathway.

Paracrine PDGF-AA from hepatocytes promotes HSC activation

Hepatocytes elicit several fibrogenic actions in a paracrine fashion to promote the activation of HSCs.[20] Thus, PCK1-mediated hepatic fibrosis may be involved in paracrine disorders. To test this hypothesis, several pro-fibrotic factors were screened, and *Pdgfa* was significantly elevated in liver tissues of L-KO mice (Figure 5A). Bioinformatics analysis confirmed that *PDGFA* were significantly increased in NAFLD and NASH patients (Figure 5B). *Pdgfa* encodes a dimer disulfide-linked polypeptide (PDGF-AA), and the chronic elevation of PDGF-AA in mice liver induces fibrosis.[21] Immunoblotting and ELISA demonstrated increased PDGF-AA expression in liver tissues and primary hepatocytes of L-KO mice (Figure 5C-E). Moreover, PDGF-AA concentration was markedly increased in the culture medium of *PCK1*-KO cells, but decreased in that of *PCK1*-OE cells treated with 0.2 mM PA (Figure 5F). Correspondingly, platelet-derived growth factor receptor alpha (*PDGFRA*), which encodes the PDGF-AA receptor, was increased in HSCs co-cultured with *PCK1*-KO cells, while decreased in HSCs co-cultured with *PCK1*-OE cells (Figure 5G). To determine whether the pro-fibrogenic effect was mediated by PDGF-AA secretion, we used a neutralizing antibody against PDGF-AA. As expected, the increase of α-SMA, COL1A1, and COL3A1 in HSCs co-cultured with *PCK1*-KO cells can be reversed by anti-PDGF-AA treatment (Figure 5H).

Reviewing transcriptome data, we found that *Pdgfa* appeared in the heat map of the PI3K/AKT pathway (Supplementary Figure 5B). IHC results showed that p-AKT (S473) was positively correlated with PDGF-AA (Figure 5I). The AKT inhibitor MK2206 significantly blocked the increase of *PDGFA* expression levels in the supernatants and cells lysates of *PCK1*-KO cells (Figure 5J and K). Taken together, these data confirmed that PCK1 deficiency promoted the expression of PDGF-AA through the PI3K/AKT pathway, and activated HSCs through hepatocyte-HSC crosstalk.

PCK1 deficiency promotes the activation of the PI3K/AKT/PDGF-AA axis by activating RhoA signaling in hepatocytes

Rho GTPases, which cycle between active GTP-bound and inactive GDP-bound conformations, are known to activate the PI3K/AKT pathway.[22-24] Considering PCK1 catalyzes the conversion of OAA to PEP, consuming GTP to generate GDP, we speculated that PCK1 deficiency may alter intracellular GTP homeostasis. To test this hypothesis, we examined several Rho GTPase protein levels in mice liver tissues and found that GTP-bound RhoA significantly increased but inactivated RhoA, p-RhoA (S188) reduced in L-KO mice (Figure 6A-6C). Consistently, after PA treatment, levels of GTP-bound RhoA decreased but p-RhoA (S188) expression increased in *PCK1*-OE cells, while *PCK1*-KO cells displayed the opposite effects (Figure 6D-6G). Next, Rhosin was used to determine whether PI3K/AKT activation is dependent on

RhoA. Immunoblotting, ELISA, and q-PCR assays showed that Rhosin blocked the increase of activated forms of AKT and PDGF-AA in *PCK1*-KO cell lysate and supernatant, as well as *ACTA2*, *COL1A1,* and *COL3A1* expression in HSCs co-cultured with *PCK1*-KO hepatocytes (Figure 6H-J). Moreover, PCK1 and p-RhoA (S188) were downregulated in NASH patient samples, while p-AKT (S473) and PDGF-AA levels were upregulated (Figure 6K). Taken together, these data indicate that PCK1 ablation stimulated the PI3K/AKT/PDGF-AA axis by activating RhoA.

Therapeutic treatment with RhoA and AKT inhibitors reduced progressive liver fibrosis *in vivo*

To explore whether blocking RhoA/PI3K/AKT could rescue the NASH phenotype in L-KO mice, Rhosin and MK2206 were used *in vivo* (Figure 7A). Treatment of L-KO mice with Rhosin or MK2206 showed improved glucose intolerance (Supplementary Figure 6A) and insulin resistance (Supplementary Figure 6B). Furthermore, the increased liver weight was also prevented (Figure 7B), whereas body weight was reduced only in the MK2206 treatment group (Supplementary Figure 6C). Additionally, Rhosin or MK2206 administration attenuated AST and ALT levels, as well as TG and FFA levels in serum and liver tissues (Figure 7C; Supplementary Figure 6D and E). Similarly, histochemistry showed reduced liver steatosis, inflammation, and fibrosis in Rhosin or MK2206 treated mice (Figure 7D; Supplementary Figure 6F), which

was confirmed by decline in liver TNF-α and IL-6 levels (Figure 7E). Additionally, α-SMA, COL1A1, COL3A1, PDGF-AA, p-AKT (S473, T308) expression and GTP-bound RhoA levels were also decreased, while the expression of p-RhoA (S188) was increased in treatment group (Figure 7F; Supplementary Figure 6G). MK2206 or Rhosin treatment also reduced the expression of genes related to inflammation and fibrosis (Figure 7G). These data suggested that the RhoA/PI3K/AKT axis plays a key role in NASH progression in L-KO mice.

Discussion

This study revealed that the hepatic gluconeogenic enzyme PCK1 plays an important role in NASH progression. The expression of PCK1 was diminished in livers from patients or mice with NASH. Moreover, deletion of PCK1 significantly exacerbated hepatic steatosis, fibrosis, and inflammation in mouse models fed NASH diet. Mechanistically, loss of PCK1 not only promotes steatosis by enhancing lipid deposition, but also induces fibrosis by HSC activation via the PI3K/AKT/PDGF-AA axis, thus promoting the progression of NASH.

Abnormal lipid metabolism is a characteristic of NAFLD and NASH. Previous studies assumed that altered lipid homeostasis was usually caused by abnormal expression of genes related to lipid metabolism.[25] However, recent studies have demonstrated that disruption of gluconeogenesis also leads to abnormal lipid metabolism. Deficiency of fructose-1,6-bisphosphatase 1 (FBP1) and glucose-6-phosphatase catalytic subunit (G6PC), key enzymes of gluconeogenesis, results in severe hepatic steatosis and hypoglycemia, indicating that suppression of gluconeogenesis could also disrupt lipid homeostasis.[26, 27] As the first rate-limiting enzyme in gluconeogenesis, it is currently not clear whether PCK1 plays a critical role in NAFLD/NASH development. In this study, we identified a robust decrease in PCK1 expression in the livers of NASH mice and NAFLD/NASH patients, causing

severe hepatic steatosis and confirming that disordered hepatic gluconeogenesis can affect lipid homeostasis.

Previous reports have shown that PCK1 expression is increased in several obesity/diabetes mouse models, such as ZDF rats, *ob/ob* and *db/db* mice, and the disease progression of NASH is positively correlated with obesity and type 2 diabetes mellitus (T2DM).[28-30] Interestingly, we found that PCK1 expression was down-regulated in diet-induced murine NASH model. Such a discrepancy might be due to the differences in animal models. The widely used rodent models of genetic forms of obesity and diabetes, such as *ob/ob* and *db/db* mice, have increased plasma glucocorticoids, which may drive PCK1 expression.[30, 31] Another explanation is that high-fat diet supplemented with high fructose/glucose in drinking water is capable of suppressing PCK1 expression, which is consistent with the previous report. [32] Furthermore, we identified ATF3, a member of the basic leucine zipper (bZIP) family of transcription factors,[33] transcriptionally repressed *PCK1* upon PA overload *in vitro* or in NASH mouse model. This is in line with previous studies suggesting that ATF3 was upregulated in NAFLD patients and murine NASH model, and could inhibit the expression of PCK1 in alcoholic fatty liver disease.[16, 34, 35] Therefore, in the current study, we found that PCK1 markedly decreased in NASH, and PA inhibited *PCK1* transcription via the upregulation of ATF3.

382 Accumulating studies using PCK1 agonists or whole-body *Pck1* knockdown
383 mice have verified that PCK1 may affect lipid metabolism.[36, 37] In the present
384 study, we found that liver-specific *Pck1* knockout induced significant hepatic
385 steatosis even under normal feeding conditions. This is a very important
386 phenomenon, since it is uncommon for a single gene ablation to cause
387 spontaneous steatosis unless a high-fat diet is used. Moreover, we observed
388 that mice with liver *Pck1* deficiency showed aggravated inflammation when fed
389 high-fat high-fructose diet, which was completely different from a previous
390 study showing that whole-body *Pck1* knockdown prevented hepatic
391 inflammation.[38] We speculate that this discrepancy is possibly due to
392 differences between diet plan and animal models, since whole-body *Pck1*
393 knockdown may have unforeseen effects on glucolipid metabolism.
394
395 Lipid accumulation is the essence of steatosis. Emerging evidence has
396 indicated that increased fatty acid uptake is associated with lipid
397 accumulation.[39, 40] In this study, genes involved in fatty acid uptake such as
398 *Cd36* and *Slc27a1* were highly expressed in L-KO mice. In addition, *Cidec,* a
399 lipid droplet-associated protein that promotes their formation, was increased
400 by both chow and NASH diets, and recently it was claimed to upregulated in
401 NALFD patients and mice, suggesting that PCK1 ablation also promotes lipid
402 droplet formation.[41, 42] Abnormal levels of metabolites also contribute to TG
403 accumulation in liver. The G3P pathway contributes to over 90% of TG

404 synthesis.[43] Since our metabolomics data showed that G3P and PA were
405 significantly upregulated in L-KO mice, we propose that PCK1 deficiency
406 promotes hepatic lipid accumulation by enhancing the expression of *Cd36*,
407 *Slc27a1,* and *Cidec* and the levels of metabolic substrates such as G3P and
408 PA. However, the exact mechanism by which PCK1 regulates G3P pathway
409 and the expression levels of *Cd36*, *Slc27a1* remains to be further explored.
410
411 Fibrosis is another characteristic of NASH and drives the transition from simple
412 steatosis to NASH. Activation of HSCs through the secretion of profibrotic
413 cytokines, such as TGF-β and PDGF, is a key event in liver fibrosis.[44] A recent
414 study identified high mobility group protein B1 (HMGB1), secreted by
415 FBP1-deficient hepatocytes, as the main mediator to activate HSCs, showing
416 the important crosstalk between hepatocytes and HSCs via paracrine
417 signaling.[26] Herein, we found that PDGF-AA was secreted by PCK1-deficient
418 hepatocytes and acted in a paracrine manner to activate HSCs. Increased
419 deposition of extracellular matrix and activation of HSCs were shown in
420 PDGFA-transgenic mice, however, the underlying mechanism mediating
421 PDGF-AA upregulation in fibrosis remains unclear. [21] Here, we demonstrated
422 that PCK1 deficiency promoted PDGF-AA secretion via activation of the
423 RhoA/PI3K/AKT pathway. Mechanistically, we hypothesize that PCK1 deletion
424 may increase intracellular GTP levels, thus promoting the activation of RhoA
425 and further activating the PI3K/AKT pathway. Based on our *in vitro* findings,

we used pharmacological AKT and RhoA inhibitors, MK2206 and Rhosin respectively, in L-KO NASH mice. Hepatic steatosis, fibrosis, and inflammation were significantly attenuated in treated mice. Although RhoA and AKT inhibitors are currently only in phase 3 trials or preclinical studies for the treatment of liver fibrosis or clinical tumors, these compounds may also have a promising therapeutic potential for NASH.[45-47]

In conclusion, this study demonstrated that hepatic PCK1 deficiency could promote lipid deposition and fibrosis in murine NASH model. Moreover, hepatic PCK1 loss activates the RhoA/PI3K/AKT pathway, which increases secretion of PDGF-AA and promotes HSC activation. AKT/RhoA inhibitors could reduce progressive liver fibrosis, providing a therapeutic window for NASH treatment.

Acknowledgements

We would like to thank Dr. T.-C He (University of Chicago, USA) and Prof. Ding Xue (Tsinghua University, China) for providing the pAdEasy and CRISPR/Cas9 system, respectively. We thank Prof. Youde Cao and Yalan Wang (Chongqing Medical University, China) for providing samples and pathological analysis support.

Grant support: This work was supported by the National Natural Science Foundation of China (grant no. U20A20392, 82073251, 82072286, 81872270), the 111 Project (No. D20028), the Natural Science Foundation Project of Chongqing (cstc2018jcyjAX0254, cstc2019jscx-dxwtBX0019, cstc2019jcyj-msxmX0587), the Major National S&T program (2017ZX10202203-004), the Leading Talent Program of CQ CSTC (CSTCCXLJRC201719), the Science and Technology Research Program of Chongqing Municipal Education Commission (KJZD-M202000401, KJQN201900429, CY200406), the Kuanren talents program of the second affiliated hospital of Chongqing Medical University, and the Scientific Research Innovation Project for Postgraduate in Chongqing (CYB19168, CYS19193).

Conflict of interest: The authors disclose no conflicts.

Transcript Profiling: Raw data were deposited in the GEO database

(GSE162211).

Author contributions: NT, AH, and KW conceived and designed the study. QY, YL and GZ performed most experiments and analyzed the data. HD, CC and KW conducted bioinformatics analysis. XP assisted with mice experiments. XW, JF, and QP provided human NAFLD/NASH samples. QY, KW, and NT wrote the manuscript with all authors providing feedback. The order of the co-first authors was assigned on the basis of their relative contributions to the study.

Abbreviations:

AKT, protein kinase B; ALT, Alanine transaminase; AST, aspartate transaminase; α-SMA, alpha-smooth muscle actin (ACTA2); ATF3, Activating Transcription Factor 3; bZIP, Basic Leucine Zipper; ChIP, chromatin immunoprecipitation; CIDEC and CIDEA, cell death inducing DFFA like effector C and A; COL1A1, COL1A3, recombinant collagen type I alpha 1 and alpha 3; CD36, fatty acid translocase; DNL, *de novo* lipogenesis; FFA, free fatty acid; G3P, glycerol 3-phosphate; GTT, glucose tolerance test; GSEA, Gene Set Enrichment Analysis; HE, hematoxylin and eosin; IHC, immunohistochemistry; ITT, insulin tolerance test; Lama2, laminin subunit alpha 2; L-KO, liver-specific *Pck1*-knockout mice; NASH, non-alcoholic steatohepatitis; NAFLD, non-alcoholic fatty liver disease; NAS, NAFLD activity score; PCK1, Phosphoenolpyruvate carboxykinase 1; PCK1, Phosphoenolpyruvate carboxykinase 1; PDGF-AA, platelet-derived growth factor AA; PI3K, phosphatidylinositol 3-kinase; PPAR, Peroxisome Proliferator-Activated Receptor; RhoA, Ras homolog family member A; SLC27A1, solute carrier family 27 member 1; TC, total cholesterol; TG, Triglyceride

References

1. Younossi Z, Anstee QM, Marietti M, et al. Global burden of NAFLD and NASH: trends, predictions, risk factors and prevention. Nat Rev Gastroenterol Hepatol 2018;15:11-20.

2. Schuster S, Cabrera D, Arrese M, et al. Triggering and resolution of inflammation in NASH. Nat Rev Gastroenterol Hepatol 2018;15:349-364.

3. Arab JP, Arrese M, Trauner M. Recent Insights into the Pathogenesis of Nonalcoholic Fatty Liver Disease. Annu Rev Pathol 2018;13:321-350.

4. **Tuo L**, **Xiang J**, **Pan X**, et al. PCK1 negatively regulates cell cycle progression and hepatoma cell proliferation via the AMPK/p27(Kip1) axis. J Exp Clin Cancer Res 2019;38:50.

5. **Xiang J**, **Chen C**, **Liu R**, et al. Gluconeogenic enzyme PCK1 deficiency promotes CHK2 O-GlcNAcylation and hepatocellular carcinoma growth upon glucose deprivation. J Clin Invest 2021 Apr 15;131(8):144703.

6. **Xu D**, **Wang Z**, Xia Y, et al. The gluconeogenic enzyme PCK1 phosphorylates INSIG1/2 for lipogenesis. Nature 2020;580:530-535.

7. Santra S, Cameron JM, Shyr C, et al. Cytosolic phosphoenolpyruvate carboxykinase deficiency presenting with acute liver failure following gastroenteritis. Mol Genet Metab 2016;118:21-7.

8. She P, Shiota M, Shelton KD, et al. Phosphoenolpyruvate carboxykinase is necessary for the integration of hepatic energy

metabolism. Mol Cell Biol 2000;20:6508-17.

9. Millward CA, Desantis D, Hsieh CW, et al. Phosphoenolpyruvate carboxykinase (Pck1) helps regulate the triglyceride/fatty acid cycle and development of insulin resistance in mice. J Lipid Res 2010;51:1452-63.

10. Hoxhaj G, Manning BD. The PI3K-AKT network at the interface of oncogenic signalling and cancer metabolism. Nat Rev Cancer 2020;20:74-88.

11. Porstmann T, Griffiths B, Chung YL, et al. PKB/Akt induces transcription of enzymes involved in cholesterol and fatty acid biosynthesis via activation of SREBP. Oncogene 2005;24:6465-81.

12. Huang X, Liu G, Guo J, et al. The PI3K/AKT pathway in obesity and type 2 diabetes. Int J Biol Sci 2018;14:1483-1496.

13. Chen J, Chen J, Huang J, et al. HIF-2α upregulation mediated by hypoxia promotes NAFLD-HCC progression by activating lipid synthesis via the PI3K-AKT-mTOR pathway. Aging (Albany NY) 2019;11:10839-10860.

14. Chi Y, Gong Z, Xin H, et al. Long noncoding RNA lncARSR promotes nonalcoholic fatty liver disease and hepatocellular carcinoma by promoting YAP1 and activating the IRS2/AKT pathway. J Transl Med 2020;18:126.

15. **Suppli MP**, **Rigbolt KTG**, Veidal SS, et al. Hepatic transcriptome signatures in patients with varying degrees of nonalcoholic fatty liver

disease compared with healthy normal-weight individuals. Am J Physiol Gastrointest Liver Physiol 2019;316:G462-g472.

16. **Fang J**, **Ji YX**, **Zhang P**, et al. Hepatic IRF2BP2 Mitigates Nonalcoholic Fatty Liver Disease by Directly Repressing the Transcription of ATF3. Hepatology 2020;71:1592-1608.

17. Allen-Jennings AE, Hartman MG, Kociba GJ, et al. The roles of ATF3 in liver dysfunction and the regulation of phosphoenolpyruvate carboxykinase gene expression. J Biol Chem 2002;277:20020-5.

18. Asgharpour A, Cazanave SC, Pacana T, et al. A diet-induced animal model of non-alcoholic fatty liver disease and hepatocellular cancer. J Hepatol 2016;65:579-88.

19. Liu XJ, Duan NN, Liu C, et al. Characterization of a murine nonalcoholic steatohepatitis model induced by high fat high calorie diet plus fructose and glucose in drinking water. Lab Invest 2018;98:1184-1199.

20. Kucukoglu O, Sowa JP, Mazzolini GD, et al. Hepatokines and adipokines in NASH-related hepatocellular carcinoma. J Hepatol 2021;74:442-457.

21. **Thieringer F**, **Maass T**, Czochra P, et al. Spontaneous hepatic fibrosis in transgenic mice overexpressing PDGF-A. Gene 2008;423:23-8.

22. Higuchi M, Masuyama N, Fukui Y, et al. Akt mediates Rac/Cdc42-regulated cell motility in growth factor-stimulated cells and in invasive PTEN knockout cells. Curr Biol 2001;11:1958-62.

559 23. **Dou C**, **Liu Z**, **Tu K**, et al. P300 Acetyltransferase Mediates
560 Stiffness-Induced Activation of Hepatic Stellate Cells Into
561 Tumor-Promoting Myofibroblasts. Gastroenterology
562 2018;154:2209-2221.e14.
563 24. **Calvayrac O**, **Mazières J**. The RAS-related GTPase RHOB confers
564 resistance to EGFR-tyrosine kinase inhibitors in non-small-cell lung
565 cancer via an AKT-dependent mechanism. EMBO Mol Med
566 2017;9:238-250.
567 25. Snaebjornsson MT, Janaki-Raman S, Schulze A. Greasing the Wheels
568 of the Cancer Machine: The Role of Lipid Metabolism in Cancer. Cell
569 Metab 2020;31:62-76.
570 26. Li F, Huangyang P, Burrows M, et al. FBP1 loss disrupts liver
571 metabolism and promotes tumorigenesis through a hepatic stellate cell
572 senescence secretome. Nature 2020;22:728-739.
573 27. Vily-Petit J, Soty-Roca M, Silva M, et al. Intestinal gluconeogenesis
574 prevents obesity-linked liver steatosis and non-alcoholic fatty liver
575 disease. Gut 2020;69:2193-2202.
576 28. Yoon JC, Puigserver P, Chen G, et al. Control of hepatic
577 gluconeogenesis through the transcriptional coactivator PGC-1. Nature
578 2001;413:131-8.
579 29. Friedman SL, Neuschwander-Tetri BA, Rinella M, et al. Mechanisms of
580 NAFLD development and therapeutic strategies. Nat Med

2018;24:908-922.

30. Samuel VT, Beddow SA, Iwasaki T, et al. Fasting hyperglycemia is not associated with increased expression of PEPCK or G6Pc in patients with Type 2 Diabetes. Proc Natl Acad Sci U S A 2009;106:12121-6.

31. Imai E, Stromstedt PE, Quinn PG, et al. Characterization of a complex glucocorticoid response unit in the phosphoenolpyruvate carboxykinase gene. Mol Cell Biol 1990;10:4712-9.

32. Lundsgaard AM, Holm JB, Sjøberg KA, et al. Mechanisms Preserving Insulin Action during High Dietary Fat Intake. Cell Metab 2019;29:50-63.e4.

33. Hai T, Wolfgang CD, Marsee DK, et al. ATF3 and stress responses. Gene Expr 1999;7:321-35.

34. **Tu C**, **Xiong H**, **Hu Y**, et al. Cardiolipin Synthase 1 Ameliorates NASH Through Activating Transcription Factor 3 Transcriptional Inactivation. Hepatology 2020;72:1949-1967.

35. Tsai WW, Matsumura S, Liu W, et al. ATF3 mediates inhibitory effects of ethanol on hepatic gluconeogenesis. Proc Natl Acad Sci U S A 2015;112:2699-704.

36. Gut P, Baeza-Raja B, Andersson O, et al. Whole-organism screening for gluconeogenesis identifies activators of fasting metabolism. Nat Chem Biol 2013;9:97-104.

37. Hakimi P, Johnson MT, Yang J, et al. Phosphoenolpyruvate

carboxykinase and the critical role of cataplerosis in the control of hepatic metabolism. Nutr Metab (Lond) 2005;2:33.

38. Satapati S, Kucejova B, Duarte JA, et al. Mitochondrial metabolism mediates oxidative stress and inflammation in fatty liver. J Clin Invest 2015;125:4447-62.

39. Miquilena-Colina ME, Lima-Cabello E, Sánchez-Campos S, et al. Hepatic fatty acid translocase CD36 upregulation is associated with insulin resistance, hyperinsulinaemia and increased steatosis in non-alcoholic steatohepatitis and chronic hepatitis C. Gut 2011;60:1394-402.

40. Doege H, Grimm D, Falcon A, et al. Silencing of hepatic fatty acid transporter protein 5 in vivo reverses diet-induced non-alcoholic fatty liver disease and improves hyperglycemia. J Biol Chem 2008;283:22186-92.

41. Langhi C, Baldán Á. CIDEC/FSP27 is regulated by peroxisome proliferator-activated receptor alpha and plays a critical role in fasting- and diet-induced hepatosteatosis. Hepatology 2015;61:1227-38.

42. **Xu MJ**, **Cai Y**, **Wang H**, et al. Fat-Specific Protein 27/CIDEC Promotes Development of Alcoholic Steatohepatitis in Mice and Humans. Gastroenterology 2015;149:1030-41.e6.

43. Alves-Bezerra M, Cohen DE. Triglyceride Metabolism in the Liver. Compr Physiol 2017;8:1-8.

625 44. Tsuchida T, Friedman SL. Mechanisms of hepatic stellate cell activation.
626 Nat Rev Gastroenterol Hepatol 2017;14:397-411.
627 45. Chien AJ, Tripathy D, Albain KS, et al. MK-2206 and Standard
628 Neoadjuvant Chemotherapy Improves Response in Patients With
629 Human Epidermal Growth Factor Receptor 2-Positive and/or Hormone
630 Receptor-Negative Breast Cancers in the I-SPY 2 Trial. J Clin Oncol
631 2020;38:1059-1069.
632 46. Schmid P, Abraham J, Chan S, et al. Capivasertib Plus Paclitaxel
633 Versus Placebo Plus Paclitaxel As First-Line Therapy for Metastatic
634 Triple-Negative Breast Cancer: The PAKT Trial. J Clin Oncol
635 2020;38:423-433.
636 47. Yoon C, Cho SJ, Aksoy BA, et al. Chemotherapy Resistance in
637 Diffuse-Type Gastric Adenocarcinoma Is Mediated by RhoA Activation
638 in Cancer Stem-Like Cells. Clin Cancer Res 2016;22:971-83.

639

640 Author names in bold designate shared co-first authorship.

Figure legends

Figure 1. PCK1 is downregulated in patients with NASH and mouse models of NASH. (A) Genes downregulated in patients with obesity (n=12), NAFLD (n=15), and NASH (n=16) from GSE126848 dataset. (B) Relative *PCK1* mRNA levels in GSE126848 and GSE89632 datasets. (C) PCK1 expression in normal individuals and patients with NASH. Scale bars: 50 μm. (D-E) mRNA and protein levels of PCK1 in the livers of WT mice fed with chow diet or NASH diet. (F-G) PCK1 mRNA and protein levels in MIHA cells treated with palmitic acid (PA) or BSA. (H) Relative levels of indicated genes in MIHA cells treated with 0.2 mM PA. (I) ChIP assays were performed in MIHA cells with or without PA treatment using an antibody against ATF3, IgG or H3. (J) Protein levels of PCK1 in MIHA cells infected with either shControl or shATF3 treated with 0.2 mM PA. Data expressed as mean ± SEM; **P* < 0.05, ** *P* < 0.01, ****P* < 0.001. *P* values obtained via 2-tailed unpaired Student's t tests or one-way ANOVA with Tukey's post hoc test.

Figure 2. PCK1 ablation accelerates inflammation and fibrogenesis in NASH model. (A) Schematic diagram of mouse model fed with NASH diet. (B-D) Body weight, GTT, and ITT were measured in WT and L-KO mice (n=11). (E) Representative gross liver morphology, whole body photo, and liver weight. (F) Serum levels of insulin, ALT and AST were measured. (G) Paraffin-embedded liver sections were stained with H&E, Sirius Red, α-SMA and F4/80. Frozen sections stained with Oil Red O. Scale bars: 50 μm. (H) Quantifications of Oil red O staining, Sirius red staining, and IHC staining. (I) NAS scores of each group. (J) Levels of TNF-α and IL-6 in liver tissues were examined using ELISA (n=8). Data expressed as mean ± SEM; **P* < 0.05, ** *P* < 0.01, ****P* < 0.001. *P* values obtained via 2-tailed unpaired Student's t tests.

Figure 3. Loss of PCK1 promotes lipid accumulation confirmed by transcriptome and metabolome. RNA sequencing was performed on livers of WT and L-KO mice fed NASH diet (n=4-5). (A) Gene ontology analysis of all significantly changed genes in top 10 biological processes. (B) Volcano plot representation of significantly up- and downregulated genes. (C) GSEA plot (left) of enrichment in “PPAR signaling pathway” signature; Heatmap (right) presentation of significantly upregulated PPAR target genes. (D-E) q-PCR and immunoblot analysis of indicated genes or protein expression in mice liver tissues. (F) Relative mRNA expression of key genes in G3P pathway (n=8). (G) Upregulated metabolites detected by untargeted metabolomics (n=6). (H) The relative level of G3P and PA in mice liver tissues (n=6). Data expressed as mean ± SEM; *$P < 0.05$, ** $P < 0.01$, ***$P < 0.001$. P values obtained via 2-tailed unpaired Student’s t tests.

Figure 4. Hepatic PCK1 deficiency leads to HSC activation via PI3K/AKT pathway. (A) Pathway enrichment analysis of significantly upregulated genes in L-KO mice. (B) GSEA plot of enrichment in PI3K/AKT pathway. (C-E) Immunoblot analysis of AKT and p-AKT (S473 or T308) in mice liver tissues or *PCK1*-OE and *PCK1*-KO MIHA cells with or without 0.2 mM PA treatment. (F) Schematic flow chart of co-culture models. (G-H) q-PCR analysis of fibrosis related gene in HSC (LX-2) cells co-cultured with *PCK1*-KO or *PCK1*-OE MIHA cells. (I-J) Western blot of fibrosis related protein in liver tissues or primary HSCs (n=3). (K) COL3A1 immunostaining in mice liver sections. Scale bars: 50 μm. (L-M) Relative mRNA expression and immunofluorescence images of *ACTA2*/α-SMA, *COL1A1* and *COL3A1* in LX-2 cells co-cultured with *PCK1*-KO MIHA cells treated with AKT inhibitor MK2206 (10 μM). Scale bars: 25 μm. Data expressed as mean ± SEM; **P* < 0.05, ** *P* < 0.01, ****P* < 0.001. *P* values obtained via 2-tailed unpaired Student's t tests or one-way ANOVA with Tukey's post hoc test.

Figure 5. Paracrine PDGF-AA from hepatocytes promotes HSC activation.

(A) Expression levels of genes related to fibrogenesis. (B) Relative *PDGFA* mRNA levels in GSE126848 and GSE89632 datasets. (C-D) PDGF-AA protein levels in liver tissue detected by Western blot and ELISA. (E) PDGF-AA protein levels in primary hepatocytes (n=3). (F) Secreted PDGF-AA levels in the conditional medium of *PCK1*-KO or *PCK1*-OE MIHA cells with 0.2mM PA treatment. (G) mRNA levels of *PDGFRA* in cell lysate of LX-2 co-cultured with *PCK1*-KO or *PCK1*-OE MIHA cells treated with PA. (H) Indicated protein level in LX-2 cells co-cultured with *PCK1*-KO MIHA cells containing nonspecific rabbit IgG or a PDGF-AA blocking antibody. (I) IHC analysis of PCK1, p-AKT (S473) and PDGF-AA in mice liver sections. Scale bars: 50 μm. (J) Levels of PDGF-AA or *PDGFA* in the conditional medium or cell lysate of *PCK1*-KO MIHA cells treated with AKT inhibitor MK2206 (10 μM). (K) Indicated protein levels in *PCK1*-KO MIHA cells treated with AKT inhibitor MK2206 (10 μM). Data expressed as mean ± SEM; **P* < 0.05, ** *P* < 0.01, ****P* < 0.001. *P* values obtained via 2-tailed unpaired Student's t tests or one-way ANOVA with Tukey's post hoc test.

Figure 6. PCK1 deficiency promotes the activation of PI3K/AKT/PDGF-AA axis by activating RhoA in hepatocytes. (A) Immunoblotting analysis of indicated protein in mice liver tissues. (B) IHC analysis of p-RhoA (S188) in mice liver tissues. Scale bars: 50 μm. (C-E) Relative levels of active RhoA were measured by G-LISA in mice liver tissues, *PCK1*-OE and *PCK1*-KO MIHA cells treated with 0.2 mM PA. (F-G) Immunoblots of p-RhoA (S188) and RhoA in *PCK1*-OE and *PCK1*-KO MIHA cells with or without 0.2 mM PA treatment. (H) Expression of indicated proteins in *PCK1*-KO MIHA cells after addition of Rhosin (30 μM). (I) Levels of PDGF-AA in the supernatant of *PCK1*-KO MIHA cells treated with Rhosin (30 μM). (J) Relative mRNA expression of *ACTA2*, *COL1A1*, and *COL3A1* in LX-2 cells co-cultured with *PCK1*-KO MIHA cells treated with Rhosin (30 μM). (K) IHC analysis of PCK1, p-RhoA (S188), p-AKT (S473), and PDGF-AA in normal individuals and patients with NASH. Scale bars: 50 μm. Data expressed as mean ± SEM; **P* < 0.05, ** *P* < 0.01, ****P* < 0.001. *P* values obtained via one-way ANOVA with Tukey's post hoc test.

Figure 7. AKT and RhoA inhibitors prevent the development of NASH *in vivo.* L-KO mice were fed NASH diet for 24 weeks, and therapeutic treatment with AKT or RhoA inhibitor was initiated at 16 weeks. (A) Schematic diagram of L-KO mice treated with DMSO (n=6), Rhosin (n=6) or MK2206 (n=5). (B-C) Representative whole body, gross liver morphology, liver weight, and serum ALT and AST. (D) Paraffin-embedded liver sections were stained with HE, or immunostained for F4/80, COL3A1 and α-SMA. Frozen sections stained with Oil Red O. Scale bars: 50 μm. (E) Levels of TNF-α, IL-6 in liver tissues. (F) Expression of indicated protein in mice liver tissues. (G) mRNA levels of genes associated with lipid metabolism, fibrogenesis, and inflammatory infiltration. Data expressed as mean ± SEM; **P* < 0.05, ** *P* < 0.01, ****P* < 0.001; n.s., not statistically significant. *P* values obtained via one-way ANOVA with Tukey's post hoc test.

Figure 1

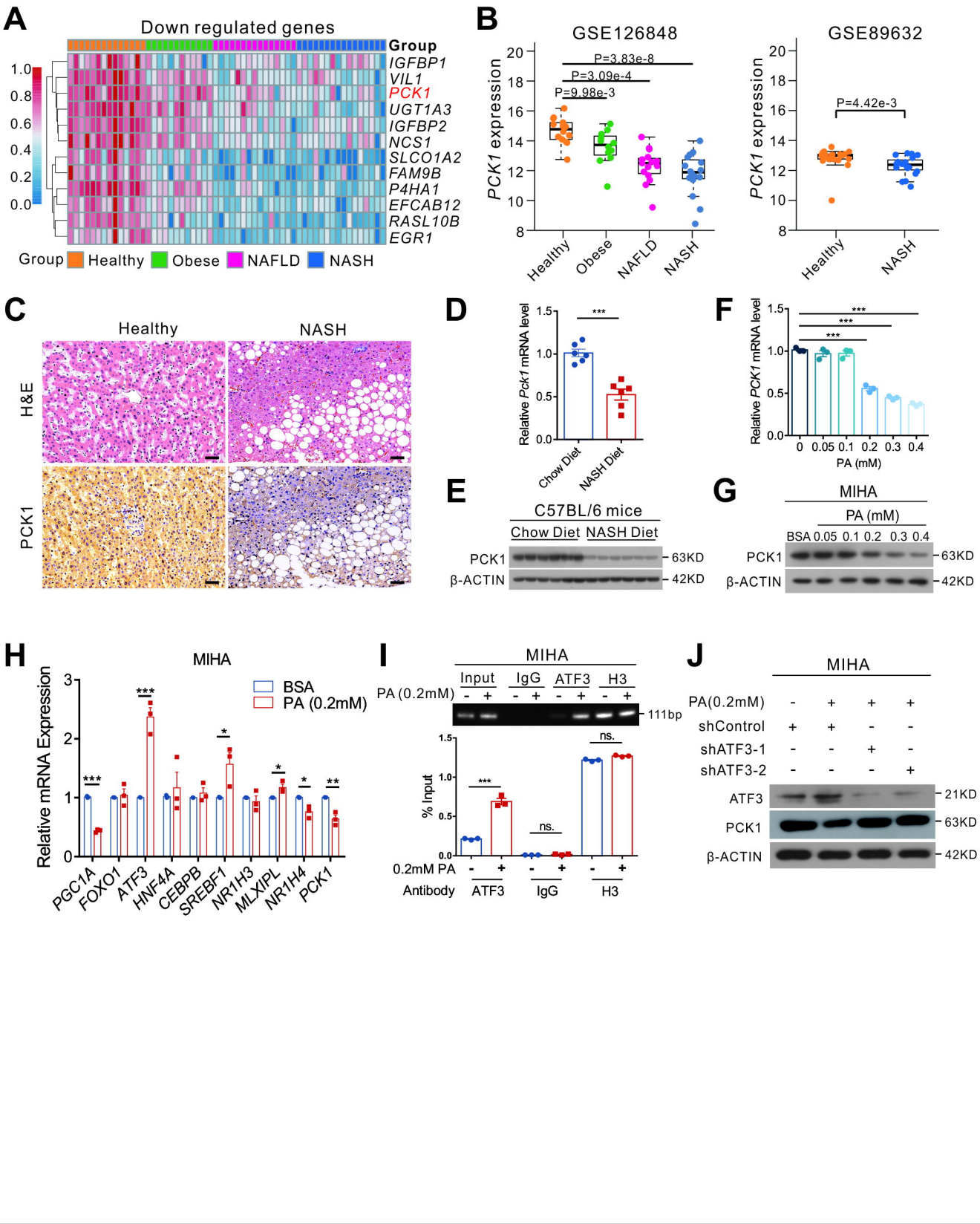
A
Down regulated genes
Group
IGFBP1
VIL1
PCK1
UGT1A3
IGFBP2
NCS1
SLCO1A2
FAM9B
P4HA1
EFCAB12
RASL10B
EGR1
1.0
0.8
0.6
0.4
0.2
0.0
Group Healthy Obese NAFLD NASH
B
GSE126848
PCK1 expression
P=3.83e-8
P=3.09e-4
P=9.98e-3
Healthy
Obese
NAFLD
NASH
GSE89632
P=4.42e-3
C
Healthy
NASH
H&E
PCK1
D
Relative Pck1 mRNA level
***
Chow Diet
NASH Diet
F
Relative PCK1 mRNA level
PA (mM)
E
C57BL/6 mice
Chow Diet NASH Diet
PCK1
β-ACTIN
63KD
42KD
G
MIHA
PA (mM)
BSA 0.05 0.1 0.2 0.3 0.4
H
MIHA
BSA
PA (0.2mM)
Relative mRNA Expression
PGC1A
FOXO1
ATF3
HNF4A
CEBPB
SREBF1
NR1H3
MLXIPL
NR1H4
PCK1
I
MIHA
Input
IgG
ATF3
H3
PA (0.2mM)
111bp
% Input
ns.
0.2mM PA
Antibody
J
MIHA
PA(0.2mM)
shControl
shATF3-1
shATF3-2
ATF3
21KD
63KD
42KD

Figure 2

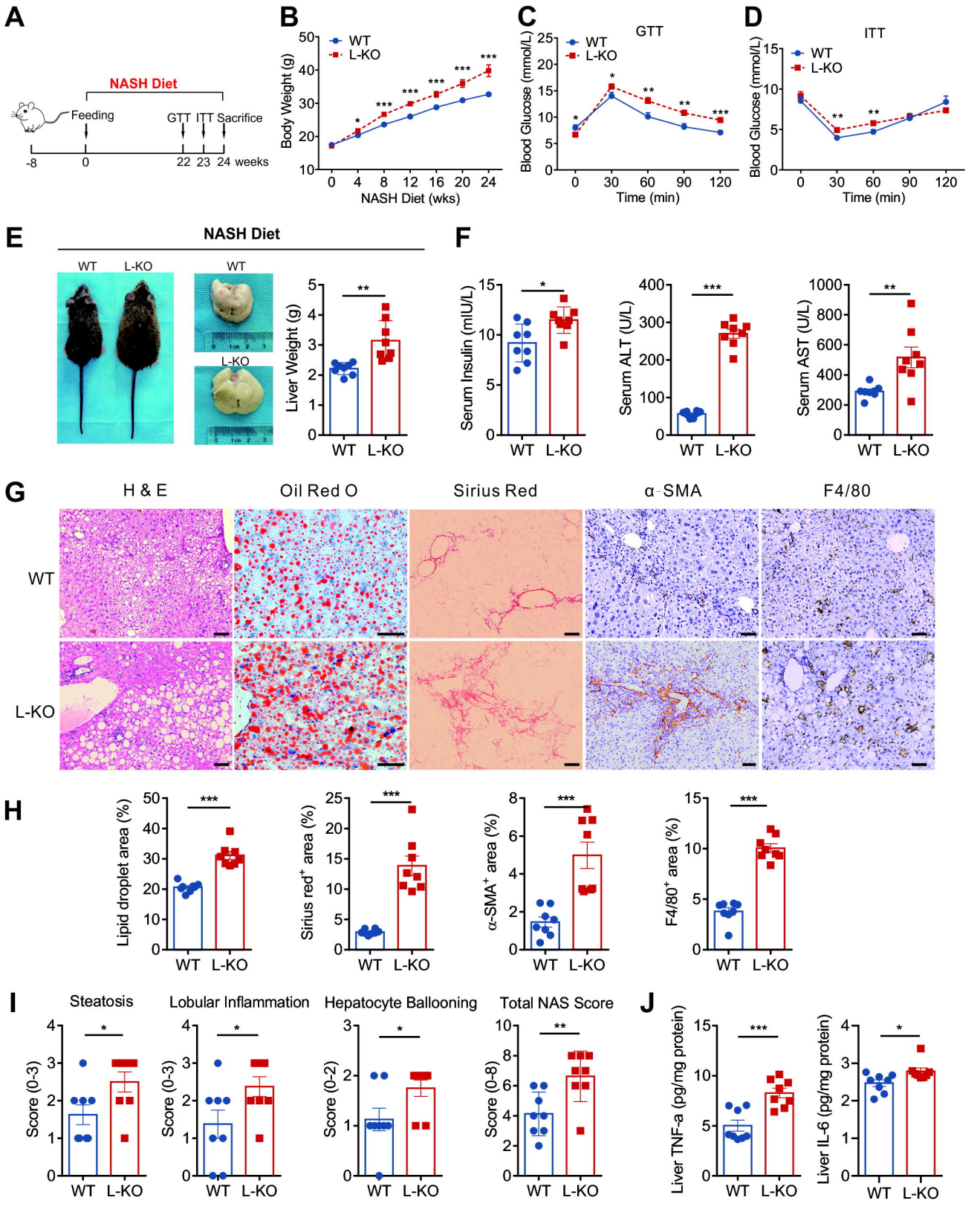
A
NASH Diet
Feeding
GTT ITT Sacrifice
-8 0 22 23 24 weeks
B
WT
L-KO
Body Weight (g)
NASH Diet (wks)
C
GTT
Blood Glucose (mmol/L)
Time (min)
D
ITT
Blood Glucose (mmol/L)
Time (min)
E
NASH Diet
WT L-KO
Liver Weight (g)
F
Serum Insulin (mIU/L)
Serum ALT (U/L)
Serum AST (U/L)
G
H & E
Oil Red O
Sirius Red
α-SMA
F4/80
WT
L-KO
H
Lipid droplet area (%)
Sirius red+ area (%)
α-SMA+ area (%)
F4/80+ area (%)
I
Steatosis
Lobular Inflammation
Hepatocyte Ballooning
Total NAS Score
Score (0-3)
Score (0-2)
Score (0-8)
J
Liver TNF-a (pg/mg protein)
Liver IL-6 (pg/mg protein)

Figure 3

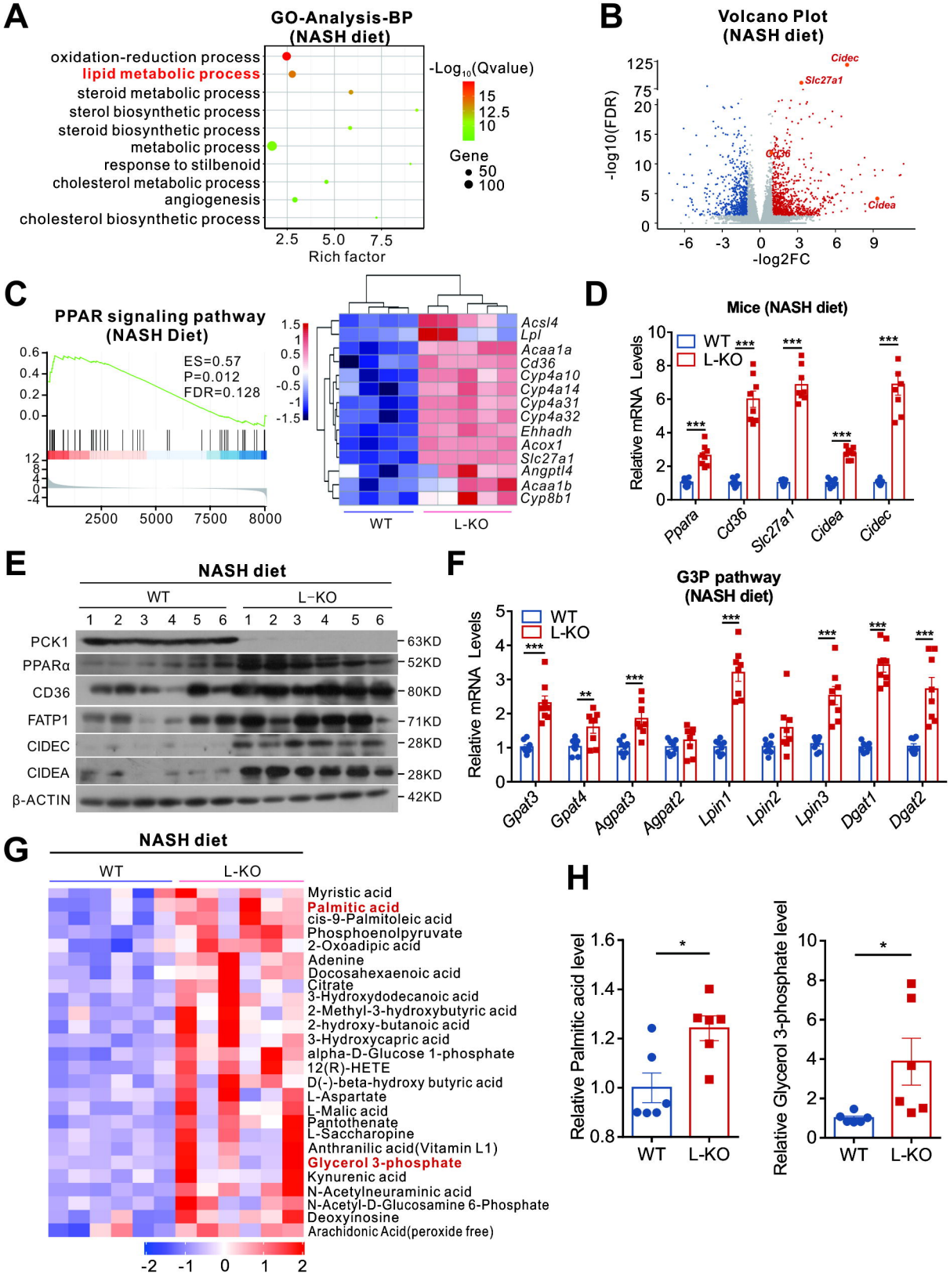
A
GO-Analysis-BP
(NASH diet)
oxidation-reduction process
lipid metabolic process
steroid metabolic process
sterol biosynthetic process
steroid biosynthetic process
metabolic process
response to stilbenoid
cholesterol metabolic process
angiogenesis
cholesterol biosynthetic process
2.5 5.0 7.5
Rich factor
-Log10(Qvalue)
15
12.5
10
Gene
50
100
B
Volcano Plot
(NASH diet)
-log10(FDR)
-log2FC
Cidec
Slc27a1
Cd36
Cidea
C
PPAR signaling pathway
(NASH Diet)
ES=0.57
P=0.012
FDR=0.128
2500 5000 7500 8000
Acsl4
Lpl
Acaa1a
Cd36
Cyp4a10
Cyp4a14
Cyp4a31
Cyp4a32
Ehhadh
Acox1
Slc27a1
Angptl4
Acaa1b
Cyp8b1
WT
L-KO
D
Mice (NASH diet)
Relative mRNA Levels
WT
L-KO
Ppara
Cd36
Slc27a1
Cidea
Cidec
E
NASH diet
WT
L-KO
1 2 3 4 5 6 1 2 3 4 5 6
PCK1
PPARα
CD36
FATP1
CIDEC
CIDEA
β-ACTIN
63KD
52KD
80KD
71KD
28KD
28KD
42KD
F
G3P pathway
(NASH diet)
Relative mRNA Levels
WT
L-KO
Gpat3
Gpat4
Agpat3
Agpat2
Lpin1
Lpin2
Lpin3
Dgat1
Dgat2
G
NASH diet
WT
L-KO
Myristic acid
Palmitic acid
cis-9-Palmitoleic acid
Phosphoenolpyruvate
2-Oxoadipic acid
Adenine
Docosahexaenoic acid
Citrate
3-Hydroxydodecanoic acid
2-Methyl-3-hydroxybutyric acid
2-hydroxy-butanoic acid
3-Hydroxycapric acid
alpha-D-Glucose 1-phosphate
12(R)-HETE
D(-)-beta-hydroxy butyric acid
L-Aspartate
L-Malic acid
Pantothenate
L-Saccharopine
Anthranilic acid(Vitamin L1)
Glycerol 3-phosphate
Kynurenic acid
N-Acetylneuraminic acid
N-Acetyl-D-Glucosamine 6-Phosphate
Deoxyinosine
Arachidonic Acid(peroxide free)
-2 -1 0 1 2
H
Relative Palmitic acid level
Relative Glycerol 3-phosphate level
WT
L-KO
WT
L-KO

Figure 4

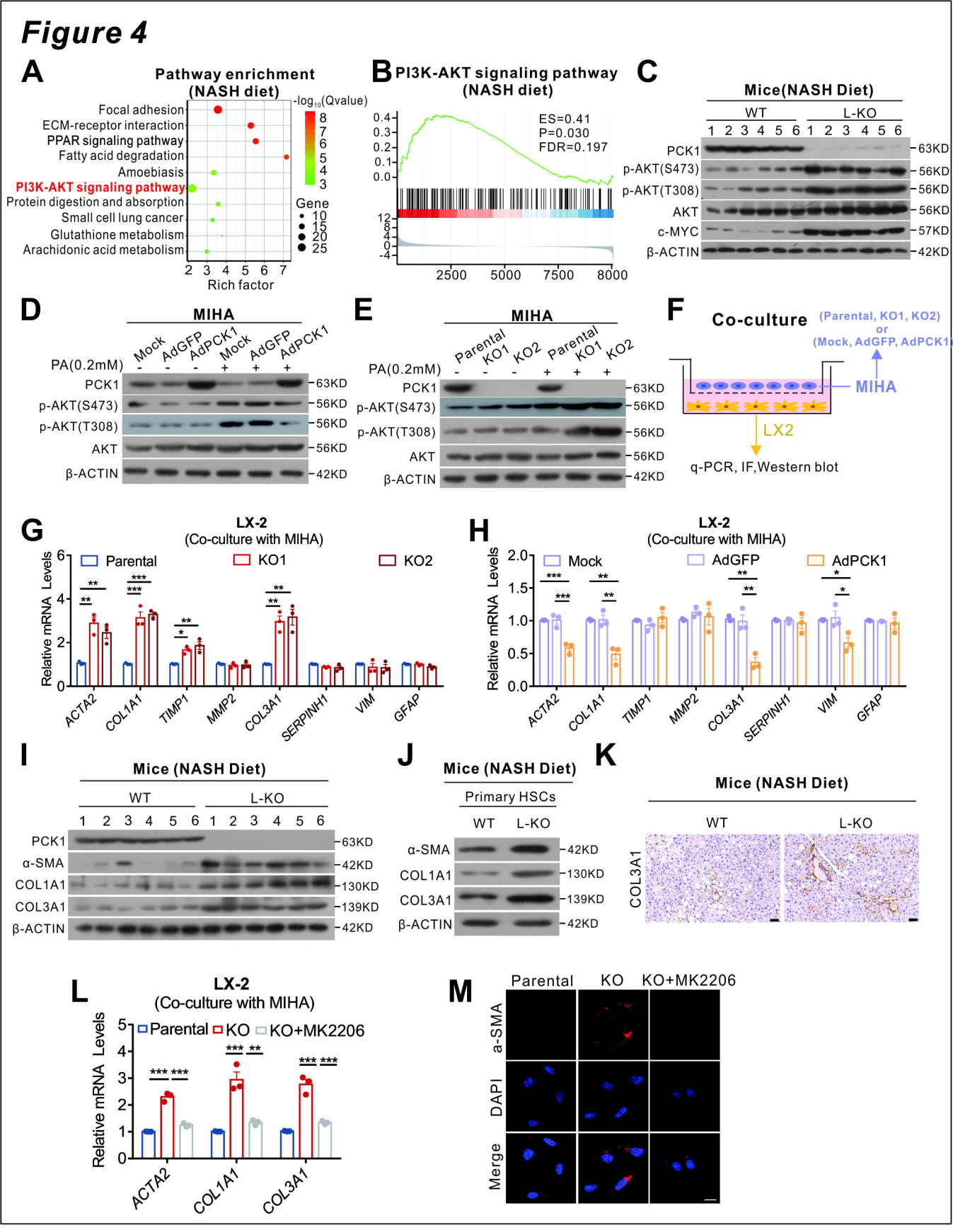
A
Pathway enrichment
(NASH diet)
-log10(Qvalue)
Focal adhesion
ECM-receptor interaction
PPAR signaling pathway
Fatty acid degradation
Amoebiasis
PI3K-AKT signaling pathway
Protein digestion and absorption
Small cell lung cancer
Glutathione metabolism
Arachidonic acid metabolism
Gene
Rich factor
B PI3K-AKT signaling pathway
(NASH diet)
ES=0.41
P=0.030
FDR=0.197
C
Mice(NASH Diet)
WT
L-KO
PCK1
p-AKT(S473)
p-AKT(T308)
AKT
c-MYC
β-ACTIN
D
MIHA
Mock
AdGFP
AdPCK1
PA(0.2mM)
E
MIHA
Parental
KO1
KO2
F
Co-culture
(Parental, KO1, KO2)
or
(Mock, AdGFP, AdPCK1)
MIHA
LX2
q-PCR, IF,Western blot
G
LX-2
(Co-culture with MIHA)
Parental
KO1
KO2
Relative mRNA Levels
ACTA2
COL1A1
TIMP1
MMP2
COL3A1
SERPINH1
VIM
GFAP
H
LX-2
(Co-culture with MIHA)
Mock
AdGFP
AdPCK1
I
Mice (NASH Diet)
α-SMA
COL1A1
COL3A1
β-ACTIN
J
Mice (NASH Diet)
Primary HSCs
K
Mice (NASH Diet)
L
LX-2
(Co-culture with MIHA)
Parental
KO
KO+MK2206
M
Parental
KO
KO+MK2206
a-SMA
DAPI
Merge

Figure 5

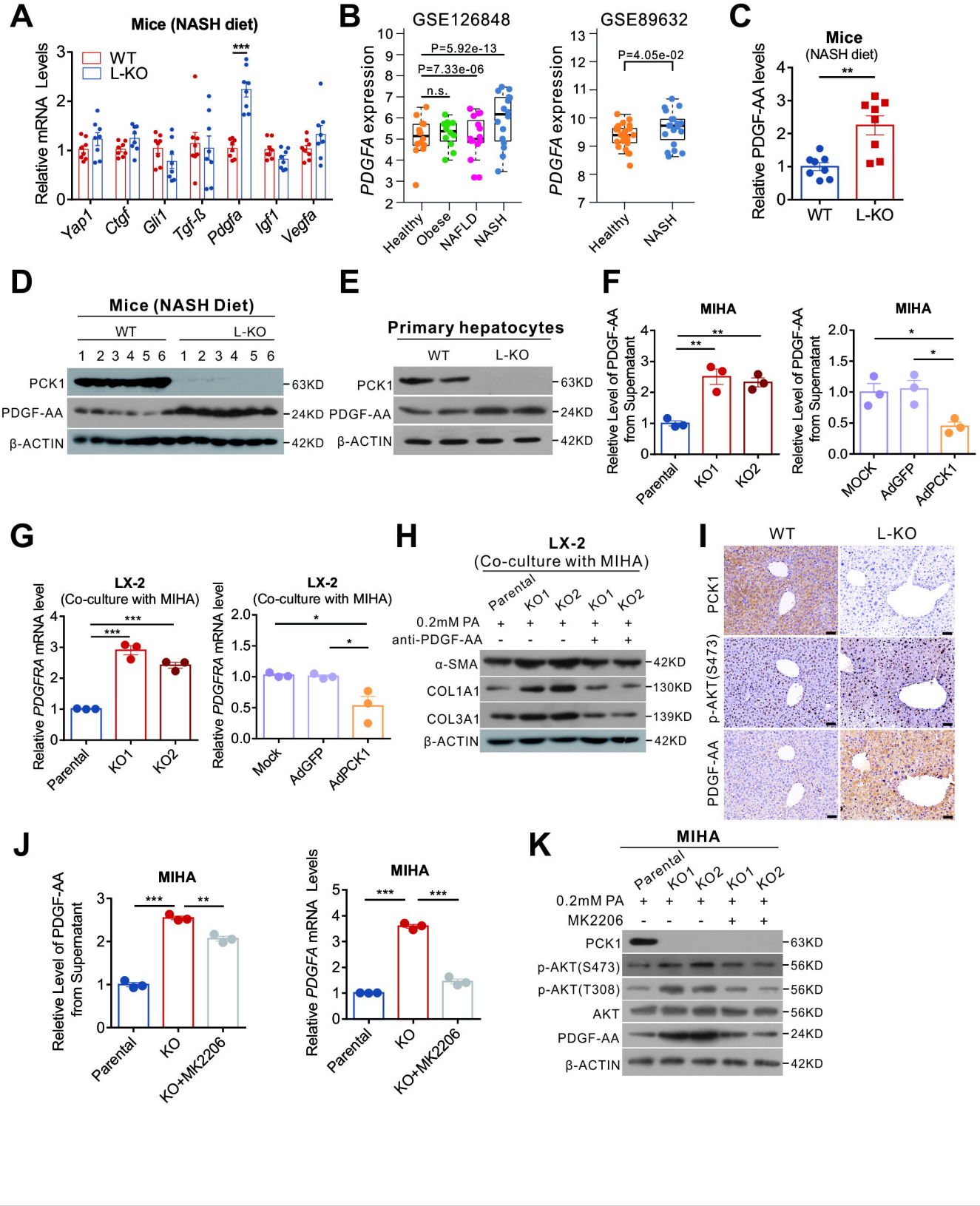
A
Mice (NASH diet)
WT
L-KO
Relative mRNA Levels
***
Yap1
Ctgf
Gli1
Tgf-ß
Pdgfa
Igf1
Vegfa
B
GSE126848
PDGFA expression
P=5.92e-13
P=7.33e-06
n.s.
Healthy
Obese
NAFLD
NASH
GSE89632
P=4.05e-02
Healthy
NASH
C
Mice
(NASH diet)
Relative PDGF-AA levels
**
WT
L-KO
D
Mice (NASH Diet)
WT
L-KO
1 2 3 4 5 6 1 2 3 4 5 6
PCK1
PDGF-AA
β-ACTIN
63KD
24KD
42KD
E
Primary hepatocytes
WT
L-KO
PCK1
PDGF-AA
β-ACTIN
63KD
24KD
42KD
F
MIHA
Reletive Level of PDGF-AA from Supernatant
**
**
Parental
KO1
KO2
MIHA
Reletive Level of PDGF-AA from Supernatant
*
*
MOCK
AdGFP
AdPCK1
G
LX-2
(Co-culture with MIHA)
Relative PDGFRA mRNA level
***
***
Parental
KO1
KO2
LX-2
(Co-culture with MIHA)
Relative PDGFRA mRNA level
*
*
Mock
AdGFP
AdPCK1
H
LX-2
(Co-culture with MIHA)
Parental
KO1
KO2
KO1
KO2
0.2mM PA + + + + +
anti-PDGF-AA - - - + +
α-SMA
COL1A1
COL3A1
β-ACTIN
42KD
130KD
139KD
42KD
I
WT
L-KO
PCK1
p-AKT(S473)
PDGF-AA
J
MIHA
Reletive Level of PDGF-AA from Supernatant
***
**
Parental
KO
KO+MK2206
MIHA
Relative PDGFA mRNA Levels
***
***
Parental
KO
KO+MK2206
K
MIHA
Parental
KO1
KO2
KO1
KO2
0.2mM PA + + + + +
MK2206 - - - + +
PCK1
p-AKT(S473)
p-AKT(T308)
AKT
PDGF-AA
β-ACTIN
63KD
56KD
56KD
56KD
24KD
42KD

Figure 6

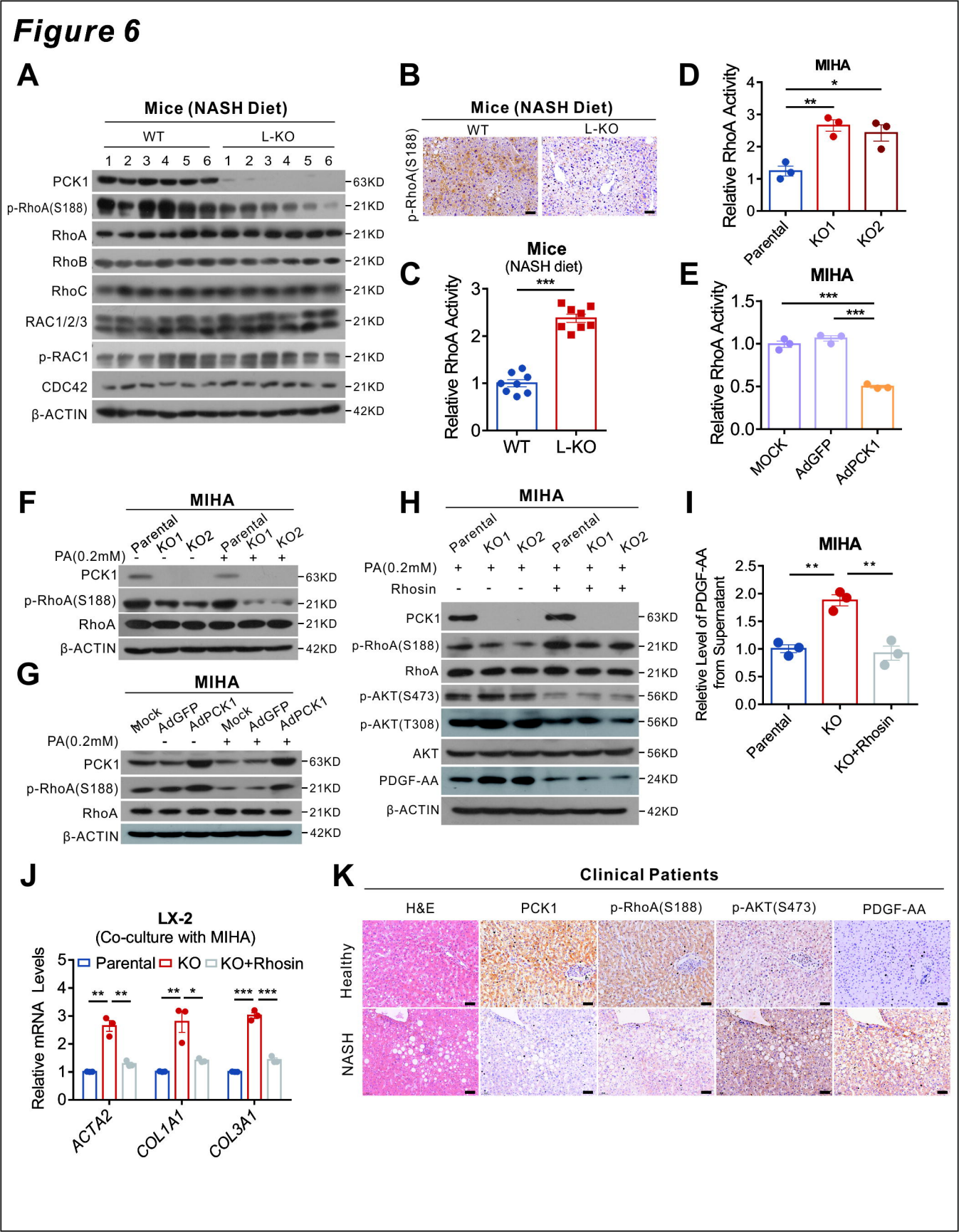
A
Mice (NASH Diet)
WT
L-KO
1 2 3 4 5 6 1 2 3 4 5 6
PCK1
p-RhoA(S188)
RhoA
RhoB
RhoC
RAC1/2/3
p-RAC1
CDC42
β-ACTIN
63KD
21KD
21KD
21KD
21KD
21KD
21KD
21KD
42KD
B
Mice (NASH Diet)
WT
L-KO
p-RhoA(S188)
C
Mice
(NASH diet)
Relative RhoA Activity
***
WT
L-KO
D
MIHA
Relative RhoA Activity
*
**
Parental
KO1
KO2
E
MIHA
Relative RhoA Activity
***
***
MOCK
AdGFP
AdPCK1
F
MIHA
Parental
KO1
KO2
Parental
KO1
KO2
PA(0.2mM)
PCK1
p-RhoA(S188)
RhoA
β-ACTIN
63KD
21KD
21KD
42KD
G
MIHA
Mock
AdGFP
AdPCK1
Mock
AdGFP
AdPCK1
PA(0.2mM)
PCK1
p-RhoA(S188)
RhoA
β-ACTIN
63KD
21KD
21KD
42KD
H
MIHA
Parental
KO1
KO2
Parental
KO1
KO2
PA(0.2mM)
Rhosin
PCK1
p-RhoA(S188)
RhoA
p-AKT(S473)
p-AKT(T308)
AKT
PDGF-AA
β-ACTIN
63KD
21KD
21KD
56KD
56KD
56KD
24KD
42KD
I
MIHA
Reletive Level of PDGF-AA from Supernatant
**
**
Parental
KO
KO+Rhosin
J
LX-2
(Co-culture with MIHA)
Relative mRNA Levels
Parental
KO
KO+Rhosin
** **
** *
*** ***
ACTA2
COL1A1
COL3A1
K
Clinical Patients
H&E
PCK1
p-RhoA(S188)
p-AKT(S473)
PDGF-AA
Healthy
NASH

Figure 7

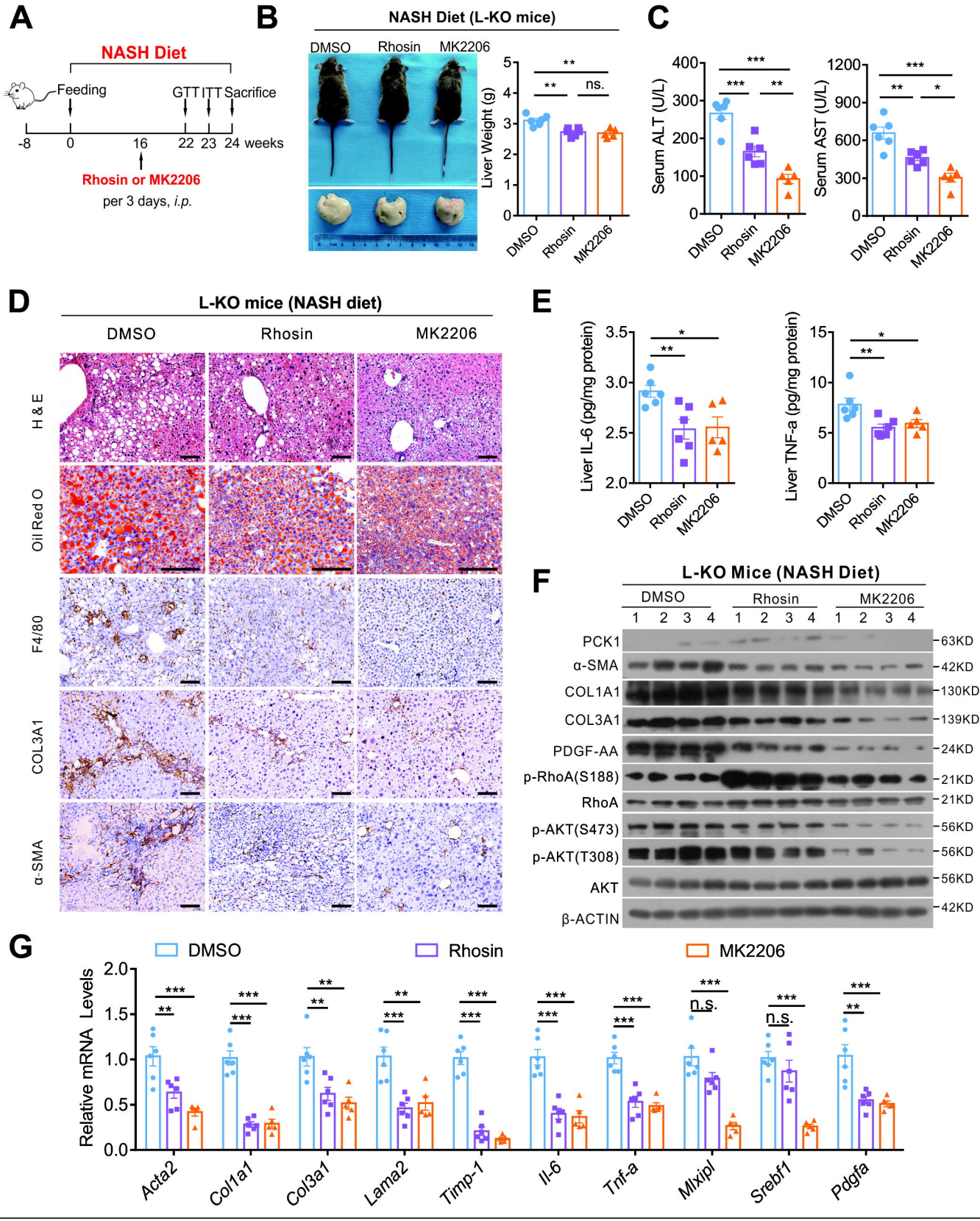
A
NASH Diet
Feeding
GTT ITT Sacrifice
-8 0 16 22 23 24 weeks
Rhosin or MK2206
per 3 days, i.p.
B
NASH Diet (L-KO mice)
DMSO Rhosin MK2206
Liver Weight (g)
ns.
C
Serum ALT (U/L)
Serum AST (U/L)
D
L-KO mice (NASH diet)
DMSO Rhosin MK2206
H & E
Oil Red O
F4/80
COL3A1
α-SMA
E
Liver IL-6 (pg/mg protein)
Liver TNF-a (pg/mg protein)
F
L-KO Mice (NASH Diet)
DMSO Rhosin MK2206
PCK1
α-SMA
COL1A1
COL3A1
PDGF-AA
p-RhoA(S188)
RhoA
p-AKT(S473)
p-AKT(T308)
AKT
β-ACTIN
63KD
42KD
130KD
139KD
24KD
21KD
21KD
56KD
56KD
56KD
42KD
G
DMSO Rhosin MK2206
Relative mRNA Levels
Acta2 Col1a1 Col3a1 Lama2 Timp-1 Il-6 Tnf-a Mlxipl Srebf1 Pdgfa
n.s.